Suppressed Superconductivity on the Surface of Superconducting RF Quality Niobium for Particle Accelerating Cavities

Z. H. Sung, A. A. Polyanskii, P. J. Lee, A. Gurevich, and D.C. Larbalestier

The National High Magnetic Field Laboratory, Florida State University, 1800 E. Paul Dirac Drive, Tallahassee, FL 32310, USA

Abstract. Significant performance degradation of superconducting RF (radio frequency) niobium cavities in high RF field is strongly associated with the breakdown of superconductivity on localized multi-scale surface defects lying within the 40 nm penetration depth. These defects may be on the nanometer scale, like grain boundaries and dislocations or even at the much larger scale of surface roughness and welding pits. By combining multiple superconducting characterization techniques including magneto-optical (MO) imaging and direct transport measurement with non-contact characterization of the surface topology using scanning confocal microscopy, we were able to show clear evidence of suppression of surface superconductivity at chemically treated RF-quality niobium. We found that pinning of vortices along GBs is weaker than pinning of vortices in the grains, which may indicate suppressed superfluid density on GBs. We also directly measured the local magnetic characteristics of BCP-treated Nb sample surface using a micro-Hall sensor in order to further understanding of the effect of surface topological features on the breakdown of superconducting state in RF mode.

Keywords: SRF, Nb, Magneto-Optical, Hall sensor, Confocal topology
PACS: 74.25.Wx

INTRODUCTION

Multi-scale surface defects like grain boundaries, surface roughness, niobium-oxide phases, and welding pits, are always present in Nb sheet processed into RF cavities and it is important to understand their impact on the surface RF superconducting properties in order to improve the performance and reliability of SRF cavities. SRF breakdown is determined at multiple scales: from the nano-scale (40-50 nm for Nb) surface layers of RF field penetration which defines the BCS surface resistance R_s, to submicron and micron scales of vortex penetration along the grain boundary network and the onset of strong RF dissipation at multiple defects and to macro-scales (mm) of heat transport through the cavity wall and thermal quench [1-2]. It has been proposed that grain boundaries (GBs) can be a major contributor to high RF field degradation by locally reducing superconducting gap (Δ) and depairing current density, J_b [3-5]. For these reasons we have investigated the influence of GBs on the superconducting properties of high purity niobium that has been treated using BCP (Buffered Chemical Polishing) and EP (Electropolishing) [6].

Symposium on the Superconducting Science and Technology of Ingot Niobium
AIP Conf. Proc. 1352, 142-150 (2011); doi: 10.1063/1.3579232

DESCRIPTION OF SAMPLE AND EXPERIMENTAL APPROACH

For our study, Peter Kneisel, Ganapati Rao Myneni and co-workers at TJNAF (Thomas Jefferson National Accelerator Facility) provided us with high purity (RRR > 250), large grain Nb sheet that was sliced from a cast ingot fabricated by CBMM. This as-received Nb sheet has a very large grain size > 10 mm, which allowed us to isolate multiple single- and bi-crystal samples for our investigation. Figure 1 shows an overview of this slice: a large single grain is located at the center of the slice and less than 20 grains lie in the circumference of the slice. In this image we have overlayed in red and cyan images of the top and bottom image of the slice so that the GBs appear thinner if there is no angular change from the top and the bottom (i.e. they are closer to the surface perpendicular). The "thicker-appearing" GBs in this detail are inclined at ~15-30° between the top and bottom surfaces. This gives us the ability to easily select samples with a range of grain boundary orientations to the surface.

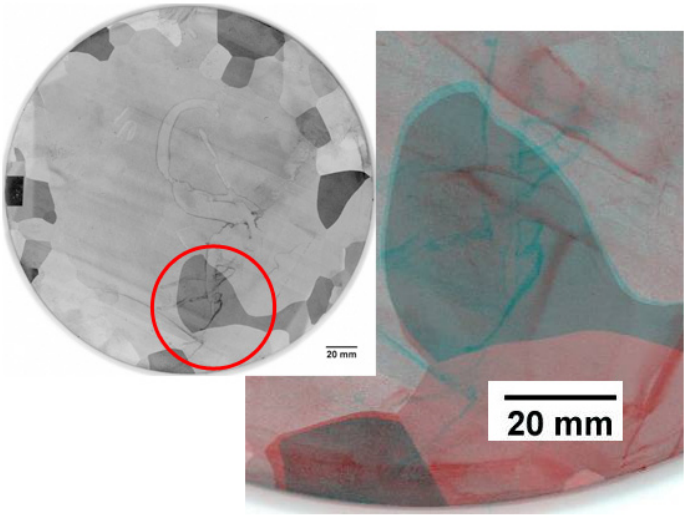

FIGURE 1. Overview of the grain structure of the ingot slice received from TJNAF (Thomas Jefferson National Accelerator Facility). The right hand image combines top (red) and bottom (cyan) surface images so as to provide with a guide to the incident angle of the grain boundaries to the sheet surface.

Previously, our work [7-9] with MOI (magneto-optical imaging) technique [10,11] showed that GBs on BCP'ed RF quality niobium bi-crystals can preferentially admit flux when GB is aligned parallel to the vector of the external magnetic field. However, understanding of topological effects produced by surface treatments on the flux penetration and fundamental understanding of angular effect shown in MO imaging were not addressed. In this study, we compared the flux penetration behavior of differently BCP and EP processed niobium bi-crystals again using MO imaging, and correlated the penetration with surface topological features examined by scanning confocal microscopy. We also investigated intrinsic properties of the grain boundaries and these bi-crystals using DC transport measurements, which had previously been developed for characterizing intrinsic GB properties and the GB depairing current density, $J_{b,gb}$, of HTS YBCO thin film [4,12,13]. We also quantified the influence of the grain boundary orientation by rotating the GB plane against the vector of magnetic

field during transport measurement. Finally, we directly measured the local magnetic field enhancement induced at the BCP'ed grain boundary surface topology using micro-Hall sensor [14].

RESULTS

Preferential Flux Penetrations at Differently Chemical-Treated GBs

To address the effect of the angle between the $\mathbf{H}_{ext}$ vector and the GB plane, we cut out two small samples from the center of a bi-crystal with a GB that was tilted away from the surface normal sufficiently that it had not previously shown preferential flux penetration at the GB (external field applied perpendicular to surface). The new samples were fabricated so that the GBs were almost perpendicular to top surface after rotating the samples by 90°. This new orientation allowed $\mathbf{H}_{ext}$ to lies in the GB plane during standard MO imaging. After mechanical thinning the sample to ~0.8-1 mm thick, a comparison was made between the samples surface treated by BCP (~60 min at <15°C, ~60 μm removed) and by EP (~2hrs, 12V at 25°C, ~60 μm removed). We quantified the topology of each surface using the contact-less technique of scanning laser confocal microscopy (SLCM), as shown in the bottom image of a) and b) in Fig. 2. Unlike the smooth surface roughness of the EP'ed bi-crystal, the BCP produced a deep (~5-7 μm) and highly inclined (~25-30°) groove at the grain boundary and local corrosion pits on the grain surface. ZFC (zero field cooled) and FC (field cooled) MO images in Fig. 2 compare the flux penetration of these two thinned BCP'ed and EP'ed bi-crystal ($\mathbf{H}_{ext}$ lies in the GB plane). As shown in Fig 2 a), for the BCP'ed bi-crystal, flux now preferentially penetrates from the both sides of the grain boundary at $H_{ext} \approx$ 58 mT, and then proceeds diagonally across the whole GB (the resolution of MO imaging, ~1-2 mT and ~5-10 μm did not allow us to measure the precise onset of penetration). Also the FC image does show evidence of some bulk current perturbation at the grain boundary. Dendritic flux penetrations and dark spots in the MO image illustrate well the effect of defects on the flux penetration [15-16]. This premature GB flux penetration is also seen on the EP'ed bi-crystal in the 72 mT ZFC MO image in Fig. 2 b). As in the BCP'ed sample, the FC mode image indicates that the bulk currents generated by vortex pinning within the whole sample were perturbed at the grain boundary.

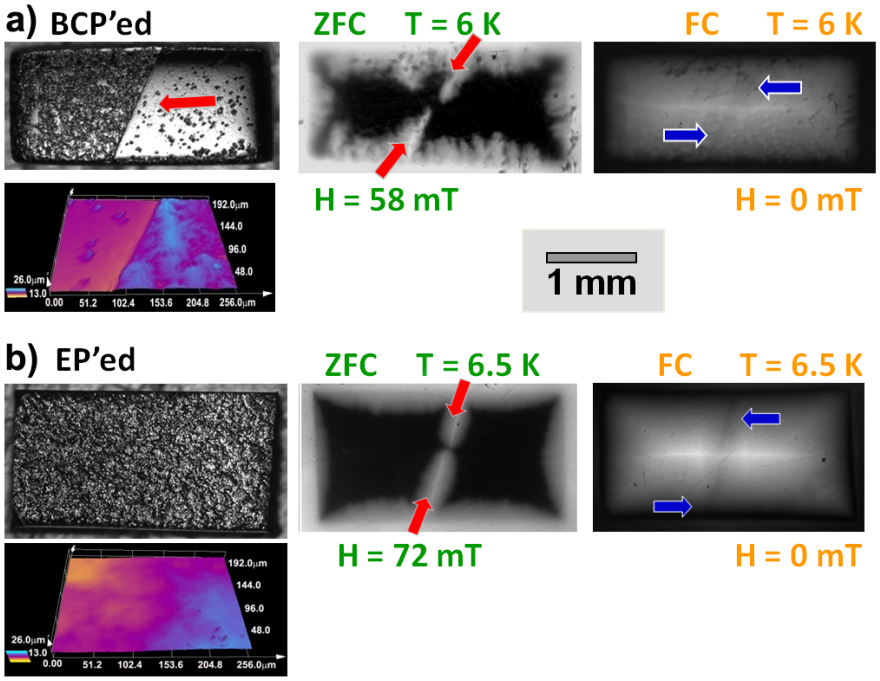

FIGURE 2. Conventional surface optical image (top) and 3D surface topological image (bottom), ZFC and FC MO images for BCP'ed bi-crystal (a) and for EP'ed bi-crystal (b). Both bi-crystals were extracted from the same grain boundary, which has a 26°crystallographic misorientation angle, in the as-received niobium sheet, but were differently chemically treated. Surface topological features of both bi-crystals were evaluated by SLCM (scanning laser confocal microscope). Red arrows in the MO image indicate the locations of preferential flux penetration along GB_{BCP} and GB_{EP} and blue arrows in the FC mode image indicate bulk current perturbation at the grain boundaries. The reflected light surface image of the BCP'ed sample shows several surface pits produced during BCP. Such pits appear also as black spots in the MO images. This EP'ed bi-crystal was prepared at 25°C, 12 V, for 2hrs.

Preferential Flux Flow at the Grain Boundary and Its Angular Dependency by DC Transport Measurement (*V-I* Characterization)

Measurement of the transport *V-I* characteristics of a single grain boundary and within a single grain required the fabrication of a very thin I-shape (dog-bone) sample. Since high purity bulk niobium samples typically have only a ~20 mT vortex domain ($H_{c1} \approx 180$ mT $< H < H_c \approx 200$ mT), it is difficult to precisely explore the change of flux pinning at grain boundary in response to external field variation. Therefore, mechanical thinning of the dog-bone sample is strongly required to reduce its original H_{c1} from H_c value, from which vortices were able to pin at the samples from earlier external field during transport measurements. After reducing the thickness, the dog-bone (I-shape) samples were BCP or EP processed in order to eliminate mechanically damaged layers. These chemical treatments produce sample surfaces with surface features representative of those found in SRF cavities. Samples were made with a single grain boundary located across the center of the dog-bone and for comparison were almost made using large single grains without grain boundaries. The full sample fabrication process is explained in detail in Ref [17].

Fig. 3a) shows the *V-J* characteristics of the BCP'ed bi-crystal sample, which has a 26° crystallographic misorientation at the GB, at 4.2K for a magnetic field applied perpendicular to the surface and thus almost in the plane of the grain boundary interface. The log *V*- log *J* curves show single-crystal-like behavior for $H_{ext} < 80$ mT but at 80 mT show a marked change, exhibiting clear evidence of a transition at a much lower I_c than the intra grain measurement. The onset field of 80 mT corresponds well to the onset of preferential GB flux flow (FF) and dissipation at low currents well below those that initiate flux flow in the grains. This *V-I* response is produced by preferential FF along the grain boundary in the range $H_{ext} = 80 – 200$ mT at much lower currents than that causes vortex motion within the grains, below I_c of intra grain. The displaced ohmic dependence $V = (I\text{-}I_b)\cdot R$ at $I \approx I_b$ defines R(H), the excess GB resistance [18]. To measure the influence of the GB orientation relative to the applied field, we performed the transport measurement while rotating the I-shape BCP'ed bi-crystal sample and its GB with respect to the external field by 0°, 30°, and 60°. The linear *V-I* response of the bi-crystal (a) in Fig. 3b) shows that the GB flux flow dissipation at $H_{ext} = 80$ mT is highly sensitive to the orientation of the GB, with dissipation greatest when the GB plane and $\mathbf{H}_{ext}$ are parallel (at 0°). The dissipation drops away markedly as the angle θ between $\mathbf{H}_{ext}$ and the GB plane increases (to 30° and 60°). The same tendency was also observed at $H_{ext} = 150$ mT; as the angle increases, the degree of dissipation by GB FF is becoming weak and finally behaves like the transition measured within a single grain.

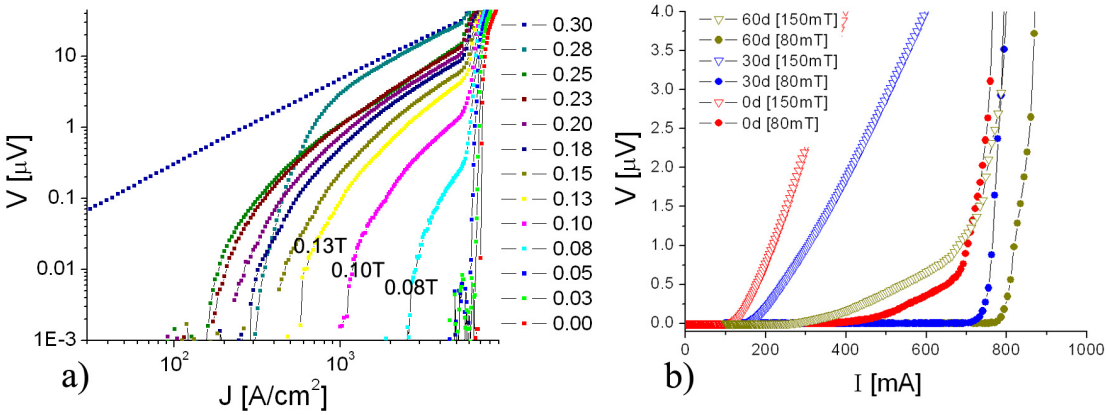

FIGURE 3. a) *V-J* characteristics of a BCP'ed bi-crystal, which has a 26° crystallographic misorientation angle at the grain boundary, at 4.2K, as a function of the external DC magnetic field. b) Linear *V-I* characteristics of this BCP'ed bi-crystal at $H = 80$ mT and $H = 150$ mT while changing of the angle between the GB plane and the vector of applied magnetic field, $\mathbf{H}_{ext}$ at 0°, 30° and 60°. This bi-crystal was BCP'ed for ~50 min to remove ~ 50 μm of cold-worked top layers after mechanically thinning up to ~100-120μm thick, then additionally BCP treated for ~50-70 min in order to further reduce their thickness. The GB plane is almost perpendicular to the sample surface. The GB has a deep and sharp GB groove on both sides (top and bottom surface) that locally reduces the sample thickness by ~ 25%.

Transport Characteristics of an EP-Treated Bi-Crystal

We also directly compared the GB flux flow behavior on the *V-I* characteristics of a BCP'ed bi-crystal (Fig. 3) with that of EP'ed bi-crystal, again ensuring that GB plane was parallel to the surface perpendicular and to $\mathbf{H}_{ext}$. Below 30-50mT field, the *V-J* characteristics in Fig. 4 shows no distinct GB flux flow behavior and the *V-I* response is similar to that of the BCP'ed single crystal. However, a non-smooth superconducting transition appears progressively above $H_{ext} \approx 100$ mT. We assume that this may be due to preferential GB flux flow. However, we can hardly find distinct linear or quasi-linear behavior by GB excess resistance even at higher external fields. Hence, we conclude that the degradation of superconductivity at the GB could be much smaller for this EP bi-crystal than for the BCP bi-crystal.

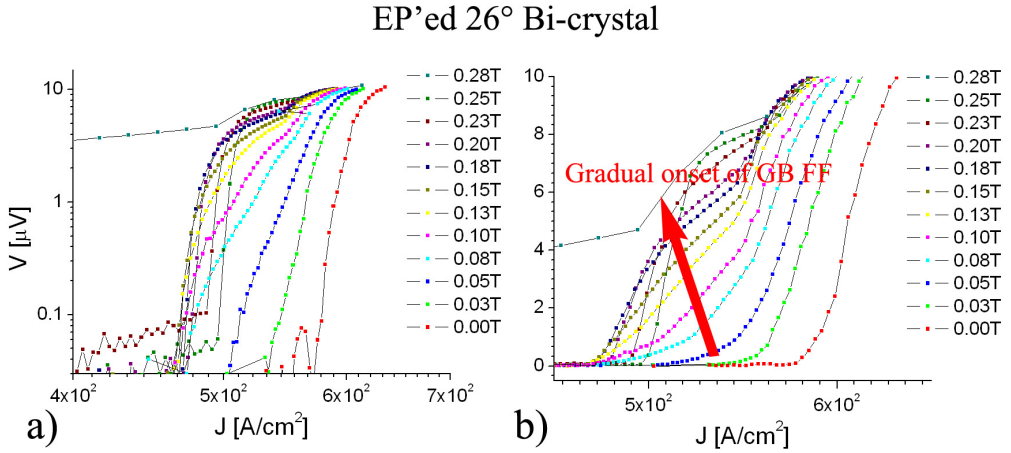

FIGURE 4. *V-J* characteristics of an EP'ed bi-crystal having 26° crystallographic misorientation angle, which was cut from the same grain boundary by BCP'ed bi-crystal (Fig. 3), in a) log-log and b) linear *V-J* scales.

Magnetic Field Enhancement at the BCP'ed Grain Boundary

Using a micro Hall-sensor that has a InSb activation area (50 × 50 μm, 5 μm thickness) on a GaAs substrate (2 × 2 mm, 0.4 mm thick), we attempted the direct measurement of the localized magnetic field enhancement [19] at a grain boundary groove produced by BCP. For this experiment, a bi-crystal was isolated from the large-grain Nb sheet (Fig. 1), then extensively chemical-treated (~100 min BCP, ~ 100 μm removed) to produce a deep and highly inclined groove at the grain boundary. This BCP'ed surface feature is shown in the surface topological image and height profile taken by SLCM, in Fig 5a. The groove is ~7-8 μm deep and ~ 140 μm wide, and its incline is characterized by a slope-change from 10.5° to 25.7° at the marked position. To measure the Hall voltage response (V_{Hall}: voltage variation on Hall sensor at constant input current (*I*) while changing external magnetic fields) which can be induced by the enhanced field at the grain boundary, we placed the micro-Hall sensor face down close to the sample surface, and then applied an external magnetic field parallel to the sample surface. In this face-down condition, the Hall activation pad was kept ~ 125 μm from the sample surface by inserting an Al_2O_3 plate between them, in

order to maintain a high V_{Hall} resolution. We compared the Hall voltage response of the grain boundary to that within the grain (which was acquired above one of the grain regions in the same bi-crystal sample, ~ 2 mm away from the grain boundary). Fig 5b) compares the behavior of the Hall voltage responses of both areas. V_{Hall} within one of the grains, as shown in the inset in detail, decreased as the external field increases, and then has a distinct kink at $H_{ext} \approx 180$ mT. This behavior indicates that there is no local field enhancement on the surface, except the field perturbation produced by the initial flux penetration on the surface at the lower critical field, H_{c1}, of niobium [20,21]. In contrast, the V_{Hall} of the grain boundary rapidly declines from that of the in-grain measurement, and then has a distinct kink, at $H_{ext} \approx 120$ mT, before $H_{c1} \approx 180$ mT. This suggests that there could be localized magnetic field enhancement on the ridge of the grain boundary region. The micro-Hall sensor has intrinsically high linearity in V_{Hall} as a function of external magnetic field so that we are able to estimate perturbed field values by inserting obtained V_{Hall} to linear line in H-V_{Hall} curve from undisturbed field measurement. We fitted linearity with V_{Hall} from the on-grain measurement at the range of $H_{ext} = 0$ mT to 180 mT (before perturbation by the onset of flux penetration at $H_{c1} \approx 180$ mT), then estimated the perturbed field values by inserting V_{Hall} induced on GB groove of the BCP'ed bi-crystal to the calibrated linear line. We found that the field enhancement at the grain boundary region is 5 to 6 times higher than in-grain, for example, at $H_{ext} \approx 50$mT, the induced field at the grain boundary, H_{gb}, is ~ 274 mT (which exceeds H_{c1} of niobium), and at $H_{ext} \approx 100$ mT, $H_{gb} \approx 635.2$ mT, which exceeds H_{c2} for Nb, which would imply that local areas of the grain boundary region are in the normal state.

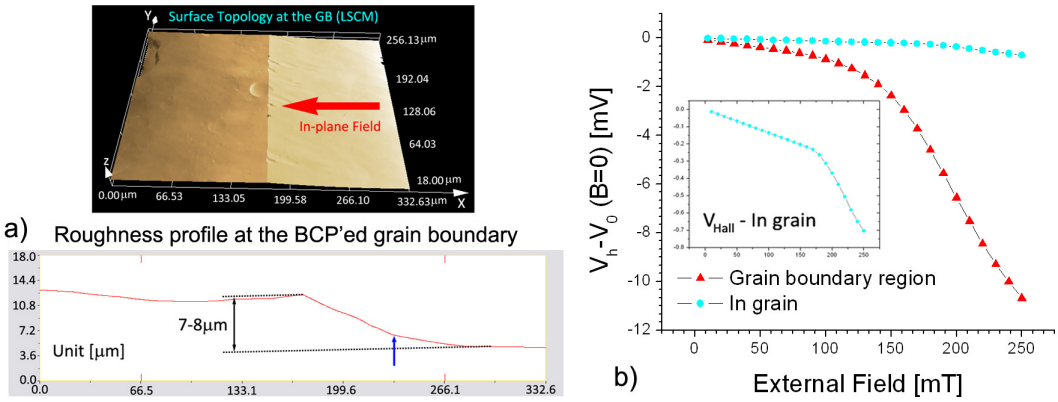

FIGURE 5. a) 3D surface topology image (top) and height profile (bottom) on BCP'ed bi-crystal that was isolated from the as-received niobium sheet (Fig.1). These images were taken by SLCM (scale is in µm). b) Comparison of Hall voltage responses between in-grain and at the grain boundary of the BCP'ed bi-crystal.

DISCUSSION

This study of the influence of the significant GB grooving produced by BCP treatment shows that the grain boundary is a weak link only if the $\mathbf{H}_{ext}$ is aligned parallel or close to parallel with the GB plane (field perpendicular to the sample surface). We also found that grooving by BCP is not the cause of preferential flux penetration when external field is aligned parallel to the GB plane since there is no

distinct difference in GB flux penetration behavior on both BCP'ed (groove) and EP'ed (no groove) bi-crystal. Similarly, by making DC transport *V-I* measurements on BCP'ed bi-crystals, we have been able to show that GBs in SRF-quality niobium prepared by BCP induce preferential flux flow when the external magnetic field lies in or close to the plane of the GB. The GB angular effect shown in this MO imaging was verified at the *V-I* transport measurements which measured GB excess resistance of BCP'ed bi-crystal while the GB plane was rotating against the vector of external field. Comparing BCP and EP we showed that for our experimental conditions EP was less deleterious to the superconducting properties of the GB than BCP. In contrast to these measurements we measured a significant enhancement of the magnetic field at a BCP'ed GB using a micro-Hall sensor when applying in-plane fields (as would be the field orientation for cavity operation), indicating that surface topological features such as those produced at grain boundaries by BCP (and at the edge of weld pits) may be sufficient to enhance the local field beyond H_{c1} and even H_{c2}. Although our multidisciplinary examinations on SRF-quality niobium show that GBs have sufficient influence on the local superconducting properties to produce breakdown of the surface superconductivity in a RF cavity, we have not yet been able to extract the GB depairing critical current density, $J_{b,gb}$, which is an important property because it can be used to describe the thermodynamic limitation of SRF niobium in RF mode. Another area that we seek to address in the future is the local microstructure and micro-chemical variation at the grain boundary produced by BCP or EP.

ACKNOWLEDGEMENTS

We would like to thank Peter Kneisel and Ganapati Rao Myneni and their colleagues at TJNAF for providing the large grain Nb ingot slice. The micro-Hall sensor was kindly provided by Dr. Milan Polak of the Institute of Electrical Engineering, Slovak Academy of Sciences, Bratislava, Slovakia. From Florida State University, we would like to thank Mr. Ian Winger for wire-EDM cutting for transport measurements. The work at the Applied Superconductivity Center was supported by the US DOE under grants DE-FG02-07ER41451, FNAL PO 570362, and the State of Florida.

REFERENCES

1. A. Gurevich, "A theoretical overview of multiscale mechanisms of RF breakdown in superconductors". Presented at Pushing the Limits of RF Superconductivity Workshop, ANL, September 22-24, (2004).
2. A. Gurevich, "Theoretical advances in SRF ". Presented at the 12th International workshop on RF Superconductivity, Cornell U., Ithaca, NY, July 10-15, 2005; Physica C **441**, 38-43 (2006).
3. A. Gurevich *et al*., *Phys. Rev. B*, 77, 104501, (2008).
4. A. Gurevich, *Phys. Rev. B*, v65, 214531, (2002).
5. J. Halbritter, *J. Appl. Phys*. **97**, 083904 (2005).
6. H. Padamsee *et al*., "RF superconductivity for accelerators" John Wiley & Sons, (1998).
7. P.J. Lee *et al*., *Phys. C*, 441 (1), 126-129 (2006)
8. P.J. Lee *et al*., "*Flux Penetration Into Grain Boundaries Large Grain Niobium Sheet For SRF Cavities: Angular Sensitivity,* Proc. Single Crystal Niobium Technology Workshop, Araxá, Brazil,

Oct. 30-Nov. 1 (2006), AIP Conf. Proc. 927, ed. G. Myneni, T. Carneiro and A. Hutton, **927**, 113-120 (2007).
9. Z.H. Sung, "Superconducting and microstructural analysis of large-grain, high-purity niobium for superconducting RF cavities" Master degree thesis, (2006).
10. A.A. Polyanskii *et al*., "Visualization of magnetic flux n magnetic materials and high temperature superconductors using the faraday effect in ferromagnetic garnet films" Tech. Phys. Lett. 15 872-873, (1990).
11. A.A. Polyanskii *et al*., "Magneto-Optical Characterization Techniques" "The Hands book on Superconducting Materials", Edited by David Cardwell and David Ginley, Institute of Physis UK, pp. 1511-1567, (2003).
12. A. Gurevich, *Phys. Rev. B*, v48, 17, (1993).
13. A. Gurevich, *Phys. Rev. Lett*. v88, No9, (2002).
14. M. Polak *et al*., "Critical Current in YBCO Coated Conductors in the Presence of a Macroscopic Defect" Applied Superconductivity, IEEE Trans. Vol 19. no3, pp. 2921-2924, (2009).
15. D.V. Denisov *et al*., *Phys. Rev. B* 73, 014512 (2006).
16. V.V. Yurchenko *et al*., *Phys. Rev. B* 76, 092504 (2007).
17. Z.H. Sung, "The influence of grain boundaries on the properties of superconducting RF (radio frequency) cavity niobium" Ph.D thesis, (2010).
18. G.A. Daniels *et al*., *Appl. Phys. Lett*. v77, n20, Nov (2000).
19. J. Knobloch *et al*., "High-Field Q slope in superconducting cavities due to magnetic field enhancement at grain boundaries", 8th SRF workshop, Santa Fe, USA (1990).
20. K. Saito, "Critical field limitation of the niobium superconducting RF cavity", KEK Accelerator Lab, , Ibaraki-ken, 10th International SRF Workshop, Japan 2001.
21. K. Saito, "Theoretical critical field in RF application" KEK Accelerator Lab, Ibaraki-ken, 10th International SRF Workshop, Japan (2001).